EAI Endorsed Transactions
on Energy Web

Research Article EAI.EU

Comparison and Validation of Five Modulation Strategies for a Dual Active Bridge Converter

Sergio Coelho[1,*], Tiago J. C. Sousa[1], Vitor Monteiro[1], Luis Machado[1], Joao L. Afonso[1] and Carlos Couto[1]

[1]ALGORITMI Research Centre, University of Minho, Guimaraes, Portugal

Abstract

This paper addresses the comparison and validation of different modulations for an isolated dc-dc dual active bridge converter (DAB), namely, Duty-Cycle Modulation, Single Phase Shift (SPS), Dual Phase Shift (DPS), Extended Phase Shift (EPS) and Triple Phase Shift (TPS). Given the DAB's applicability in a wide variety of power electronics branches, several control strategies are being studied to improve its efficiency, by mitigating circulating currents and reactive power. Regardless of the chosen architecture, appropriate modulations must be adopted, assessing which one presents the better cost-benefit ratio. This simulation-based analysis aims to investigate the DAB performance when controlled by the above-mentioned modulations and operating with a nominal power of 3.6 kW. Thus, simulation results show that only SPS, DPS, and TPS are considered suitable, while Duty-Cycle Modulation has time limitations during power transfer and EPS is more appropriate for dynamic power applications.

Keywords: Dual Active Bridge Converter, Duty-Cycle Modulation, Single Phase Shift, Dual Phase Shift, Extended Phase Shift, Triple Phase Shift.

Received on 09 November 2021, accepted on 15 February 2023, published on 22 February 2023,

doi: 10.4108/ew.v9i6.3066

1. Introduction

The dual active bridge (DAB) converter was introduced by Rik de Doncker in 1991 with the application purpose in medium/high power applications [1]. As it is possible to observe in Figure 1, its architecture is considered reasonably simple and symmetrical, in which two H-bridges are connected by a high-frequency (HF) transformer. Compared to other isolated dc-dc converter topologies, e.g., dual half-bridge and full-bridge forward (covered in [1] and [2], respectively), many advantages can be obtained. In addition to bidirectional operation, galvanic isolation, and voltage regulation, common to all topologies, soft-switching capacity is also considered through the entire power range and more degrees of freedom can be also included in the control algorithms.

*Corresponding author. Email: sergio.coelho@algoritmi.uminho.pt

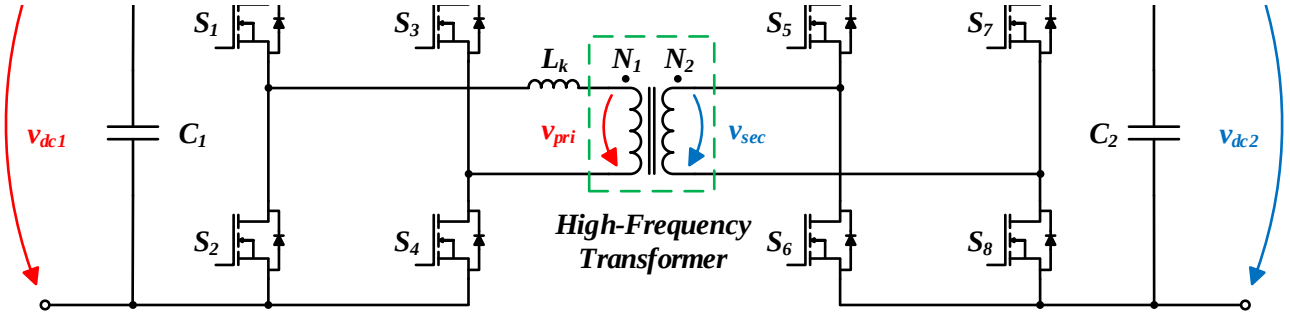

Figure 1. Dual active bridge (DAB) converter.

Since the DAB converter operates in a HF regime, its passive components have less volume and weight, namely the power transformer and the leakage inductance (L_k) which leads, consequently, to a power density increase [3]. Additionally, compared to the use of low-frequency transformers, the propagation of electromagnetic interference will also be reduced [4]. In this regard, given the latest advances in silicon carbide (SiC)-based switching devices, new magnetic core materials and digital signal processors, the use of the DAB converter has been spread to several power electronics branches [5], [6]. Besides medium/high power applications, this isolated dc-dc converter is used to interface energy storage systems, in the design of electric vehicle (EV) battery charging stations [7], mitigation of power quality problems [8], solid-state transformers [9], power electronics traction systems [10], hybrid ac-dc microgrids [11], [12], among others.

Given the growing proliferation of this isolated dc-dc converter in the most diverse power electronics branches, new DAB-based topologies have emerged in the literature. Among several examples, are highlighted: the three-level DAB converter with five control degrees of freedom [13], the neutral point clamped DAB converter [14], the multilevel DAB converter utilizing an LCL filter at the transformer side [15], and the dual bridge series resonant converter [16], which, compared to the traditional DAB, has as main features two resonant tanks and a tapped-transformer to increase the soft-switching range of the converter. Moreover, in [17], the feasibility of connecting two DAB converters in parallel is studied, so that the efficiency of the system is optimized for different voltage and power demand levels.

In addition of using new topologies that further increase the efficiency of this isolated dc-dc converter, the choice of the correct modulation techniques assumes a critical role in the operation of the DAB converter. In low power systems, in which it is necessary to dynamically regulate current and voltage in the face of transient states and oscillations, the above-mentioned modulation techniques will maintain the DAB total losses (P_t) as low as possible. Thus, in [18] a dynamic algorithm capable of controlling all the semiconductors independently is presented, in which each the duty-cycle value is altered according to the oscillations and transients. Consequently, current offsets may be mitigated (both the current that flows through the leakage inductance (i_{Lk}) and the transformer magnetization current), as well as peak currents in the semiconductors. Similarly, in [19] the implementation of a linear quadratic regulator control based on linear matrix inequalities is considered for application when there is great uncertainty in the operating parameters of the system.

Normally, DAB's efficiency increase is directly related to the reduction of reactive power and circulating currents, as well as to the adoption of new generation semiconductors and core materials (with higher saturation flux density). In this regard, in [20], issues related to transformer saturation and current peaks in systems that demand fast dynamic response are addressed. In [21], methods to attenuate current stress in each semiconductor of the DAB converter are studied. On the other hand, in [22], a modulation technique with four degrees of freedom that aims to minimize the total system losses is implemented and validated, in which soft-switching throughout the entire range of the DAB was considered and minimum-tank-current strategies were adopted to reduce reactive power. Similarly, in [23] and [24], a voltage offset is introduced to the dc blocking capacitors to reduce i_{Lk}.

Nonetheless, regarding its ease of implementation, power flow and regulation to and from each side of the DAB converter is commonly carried out by a (traditional) single phase shift (SPS) modulation. However, and as already mentioned, high values of reactive power and circulating currents may be generated, thus making it difficult to achieve zero voltage switching (ZVS). Thus, it is crucial to study methods and conditions that aim to expand the ZVS operating range. In [25] is studied a control technique capable of overcoming severe energy efficiency limitations that arise when the DAB input voltage (v_{dc1}) does not match n v_{dc2}, with n representing the transformation ratio of the HF transformer and v_{dc2} the DAB output voltage. On the other hand, in [26], a modulation technique for applications with a wide v_{dc1}/v_{dc2} voltage range is presented. The impact of dividing the leakage inductance (L_k) in the ZVS operating range is addressed in [27], while, in turn, to expand it, a control strategy for high-voltage applications is presented in [28]. Lastly, in [29], the use of a dual-transformer-based DAB is considered and studied.

The reduction of the semiconductor high-current stress and expansion of the ZVS operating range can also be achieved by increasing the number of control degrees of freedom, i.e., by implementing one of three phase shift modulation strategies: dual phase shift (DPS), extended phase shift (EPS), and triple phase shift (TPS). Comparing the four above-mentioned modulations (SPS, DPS, EPS, and TPS), the main difference lies on the value assigned to each of the phase angles, either between the two H-bridges (outer phase angle, D_0) or between the legs of each bridge (inner phase angles, D_1 and/or D_2). Depending on the chosen modulation, the efficiency of the DAB converter will vary, however, the implementation difficulty will also be different.

To compensate faults, reactive power, and possible fluctuations, new modulation techniques, derived from the four above-mentioned, are emerging. In [30] and [31], EPS and TPS derivations are presented, both aiming to suppress the occurrence of transient dc bias. In [32] and [33], an improved/cooperative TPS modulations to mitigate dual-side circulating currents are addressed. A new DPS variant is considered in [34]. In [35], a unified phase shift modulation for dynamic systems is proposed, whose main objective is to reduce peak currents during, e.g., voltage fluctuations. In [36], an SPS derived modulation is exposed. In [37], a novel hybrid current modulation is presented, based on triangular and trapezoidal current modulation techniques, aiming to reduce THD problems without increasing semiconductor stress.

In the literature, despite already existing comparative studies between the above-mentioned phase shift modulation strategies [38], [39] no reference addresses the five techniques simultaneously, which represents the main contribution of this paper. Moreover, it is important to assess the behaviour of the converter when operating as a single active bride (SAB) converter – one H-bridge switching, while the other assuming a passive behaviour (with the diodes providing the path for the current).

In this regard, this paper is organized as follows: Section 1 introduces the objective of this paper and contemplates a review on the current state-of-the-art. Section 2 indicates the operating parameters of the DAB converter. Section 3 describes and presents the simulation results for each of the five modulation techniques. Lastly, Section 4 presents the main conclusions and future work.

2. Operating Parameters of the Proposed DAB Converter

As mentioned, a certain modulation technique may be considered more or less appropriate given the application scenario. Thus, the main parameters of the DAB converter and respective values are shown in Table 1. To approximate the performed computational simulations from the real application case, the parameters will remain constant independently of the chosen modulation.

The assignment of a high value for the switching frequency (f_{sw} = 100 kHz) allows to compact the system since it reduces the volume and weight of inductors, capacitors, and transformer. On the other hand, the value of L_k was selected in order to obtain the best compromise between the expansion of the ZVS range and the DAB total losses. As (1) demonstrates, they are the result of the sum of conduction losses (P_{cond}), switching losses (P_{sw}), transformer losses (P_{tr}), and losses in L_k (P_{Lk}).

$$P_t = P_{cond} + P_{sw} + P_{tr} + P_{Lk} \quad (1)$$

Table 1. DAB converter operating parameters

Parameter	Value	Unit
Primary side dc-link voltage, v_{dc1}	400	V
Secondary side dc-link voltage, v_{dc2}	200	V
Nominal operating power	3600	W
Switching frequency, f_{sw}	100	kHz
Sampling frequency, f_s	50	kHz
Transformation ratio, n	2:1	-
Leakage inductance (primary), L_k	3.5	µH
Primary side dc-link capacitor, C_1	1680	µF
Secondary side dc-link capacitor, C_2	1680	µF
Secondary side resistive load	11.11	Ω

3. Simulation and Validation of Each Modulation Technique

As mentioned, the comparison between each modulation technique is based on computer simulations. For all cases, voltage and current waveforms will be compared, as well as the gate signals of semiconductors S_1, S_3, S_5, and S_7, considered essential to the detailed study presented in this paper.

Initially, in section 3.1, the converter operation as a SAB topology under duty-cycle modulation will be verified, presenting, in the following sections, the comparison between the four phase shift modulation techniques (SPS, DPS, EPS, and TPS).

Regardless of the chosen phase shift modulation and power flow direction, all semiconductors are always switching with a fixed 50% duty-cycle. However, it is the voltage waveform mismatch (φ) at the HF transformer terminals (v_{pri} and v_{sec}) that allows the transfer of power to and from each side of the DAB converter. Thus, v_{pri} and v_{sec}, when phase shifted, generate a voltage in L_k, and, consequently, a certain current will flow through it (i_{Lk}). Depending on whether φ is positive or negative, the direction of i_{Lk} will change and the power will flow in accordance. If v_{pri} is ahead of v_{sec}, the power will flow from the primary to the secondary side. As expected, if v_{pri} is lagged in comparison with v_{sec}, the power will flow from the secondary to the primary side of the DAB converter. It is the value of φ that regulates the transfer of power, i.e., the higher φ, the greater the transferred power. Nonetheless, for simplicity reasons, this paper only

analyzes the power flow from the primary to the secondary side of the DAB converter.

As aforementioned in the introduction, the expansion of the ZVS range is achieved by considering more degrees of freedom in the control algorithm. SPS modulation has only one degree of freedom (D_0), DPS and EPS consider two degrees of freedom (D_0 and D_1), and, lastly, TPS is the only modulation that introduces three degrees of freedom (D_0, D_1, and D_2). Normally, the value of D_0 controls the direction and the value of the transferred power to and from each side of the DAB converter, while D_1 and D_2 regulate and expand the ZVS range and minimize the circulating current, reactive power, and current peaks.

3.1. Single Active Bridge (SAB) Operating Under Duty-Cycle Modulation

The SAB converter is a well-known unidirectional isolated dc-dc topology due to its greater simplicity and robustness. By applying a duty-cycle modulation to one of the H-bridges (whilst the other assumes a passive behaviour), a moderated efficiency is provided to this conversion stage. Notwithstanding, a large snubber capacitance is used to lower switching and conduction losses, which constitutes one of the major drawbacks of the SAB. In this particular case, and as seen in Table 1, it is intended to regulate the voltage on the secondary dc-link (v_{dc2}) at 200 V, the previously established reference. To this end, a PI control algorithm is employed, in which its output will directly act on the duty-cycle value of semiconductors S_1 and S_3, as it is possible to observe in Figure 2.

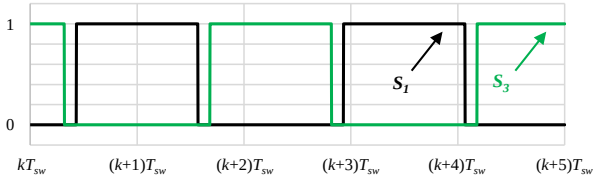

Figure 2. Triggering gate signals of S_1 and S_3 when the SAB operates under duty-cycle modulation.

Therefore, to assess the steady-state operation of the SAB converter under duty-cycle modulation, the current and voltage waveforms in the HF transformer were monitored when $v_{dc2} \approx 200$ V. As seen in Figure 3 (a), the currents in the primary and secondary sides of the HF transformer (i_{pri} and i_{sec}, respectively), despite presenting peak values of 17.51 A and 35.02 A, have null mean value and are in phase with v_{pri} and v_{sec}. Additionally, it is concluded that i_{pri} always assumes half the instantaneous value of i_{sec}, thus respecting the value of n.

By analyzing Figure 3 (b), it is shown that v_{pri} and v_{sec} assume, respectively, maximum and minimum values of ±400 V and ±200 V, which validates the veracity of the applied control algorithm. Moreover, it is also possible to conclude that v_{sec} is representative of the reflection of v_{pri} on the secondary side, however, due to v_{Lk}, a small mismatch between these voltage waveforms is verified. The lower the value of L_k, the lower v_{Lk}, the aforementioned mismatch, and the current peaks in the HF transformer.

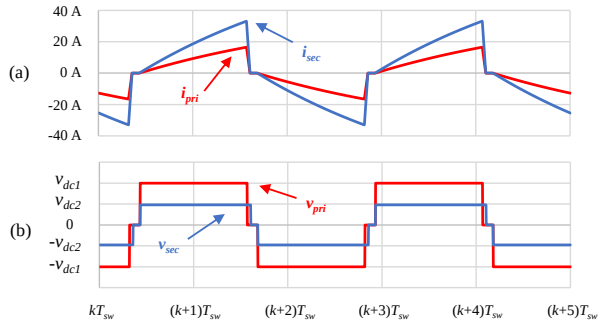

Figure 3. Waveforms in the primary and secondary sides of the HF transformer when the SAB operates under duty-cycle modulation: (a) Current; (b) Voltage.

Figure 4 shows, respectively, the waveforms of the current in the resistive load (i_{load_sec}) and of v_{dc2}. As observed, i_{load_sec} has a mean value of 17.255 A and v_{dc2} of 191.8 V, which justifies the operating power value slightly below the previously established reference of 3.6 kW.

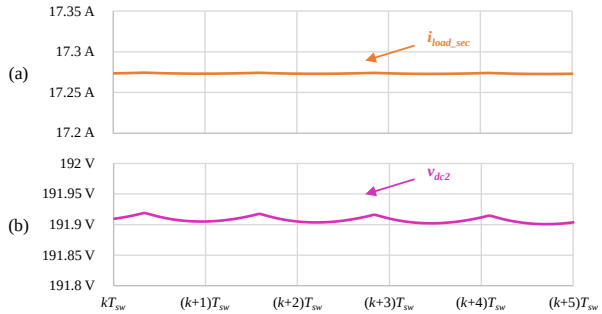

Figure 4. Waveforms in the secondary side resistive load when the SAB operates under Duty-Cycle Modulation: (a) Current; (b) Voltage.

3.2. Single Phase Shift (SPS)

Due to its simplicity, SPS is the most commonly employed modulation technique in DAB-based power converters. Nonetheless, when the value of v_{dc1} does not match $n \cdot v_{dc2}$, SPS is not considered suitable since only one degree of freedom is deemed (D_0). Consequently, such scenario leads to higher reactive power and circulating currents, which increases P_t and current peaks in the semiconductors.

In this regard, for the case of SPS modulation, the higher the value of φ, which in the SPS case equals to D_0, the greater will be the transferred power to and from each side of the DAB converter. This fact is proven by the analyses of Figure 5, in which an increase in the power value is verified as D_0 also increases ($0 \leq D_0 \leq \pi/2$). Moreover, it is also seen that the nominal power (P_N) for which the DAB converter was designed is reached when D_0 is approximated $\pi/6$ rad.

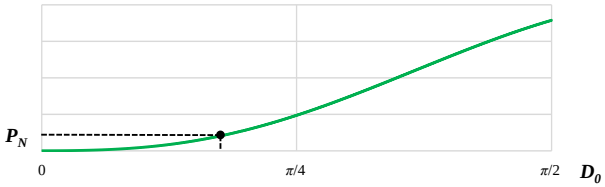

Figure 5. DAB power transfer during SPS modulation considering an increase of D_0.

For the given operating parameters, a PI control algorithm is used to approximate v_{dc2} to its reference value (200 V). As observed in Figure 6 (a), v_{pri} and v_{sec} waveforms present two voltage levels ($+v_{dcx}$ and $-v_{dcx}$) since only one degree of freedom is deemed (D_0). Additionally, and as shown in detail in Figure 6 (b), it is also concluded that v_{pri} is ahead of v_{sec} (positive φ), which is indicative of the power flow direction, i.e., from the primary to the secondary side of DAB. Note that such value of φ, i.e., D_0, is generated by the PI control algorithm.

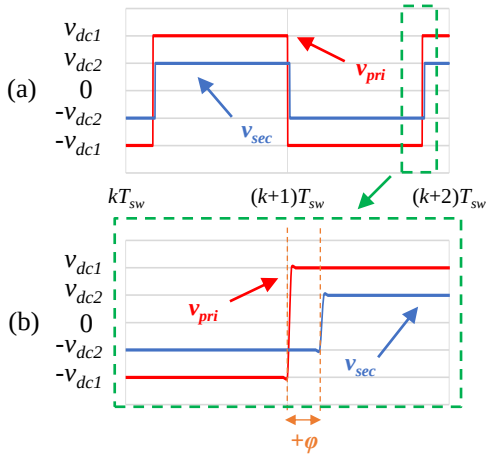

Figure 6. Voltage waveforms in the primary and secondary sides of the HF transformer using SPS modulation: (a) During a full cycle; (b) In detail.

Regarding i_{pri} and i_{sec}, by observing Figure 7, it is seen that their mean value is null and that they are in accordance with v_{pri} and v_{sec}, as in the SAB converter operating under duty-cycle modulation. In other words, the currents have a positive value when the voltage is positive, the same happening for negative values.

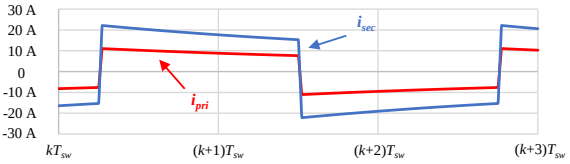

Figure 7. Current waveforms in the primary and secondary sides of the HF transformer using SPS modulation.

The voltage and current waveforms in the resistive load connected in parallel with the secondary dc-link are presented in Figure 8. In steady-state, the mean value of v_{dc2} is 199.03 V and of i_{load_sec} is 17.92 A, which represents an approximate active power of 3.57 kW, i.e., 30 W below its reference value.

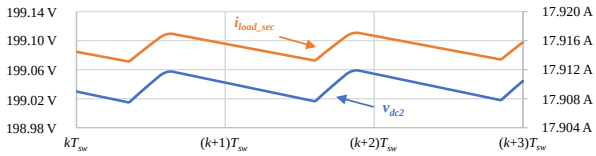

Figure 8. Voltage and current waveforms in the secondary side resistive load using SPS modulation.

As aforementioned, the SPS modulation technique only deems one degree of freedom, i.e., the outer phase angle D_0, observed in Figure 9 (b). Since the inner phase angles D_1 and D_2 are not considered, S_1 and S_3 are 180° phase shifted (Figure 9 (a)), as well as S_5 and S_7. Given that the presented triggering gate signals were captured in steady-state, the value of D_0 (and, in this case, of φ) is relatively low – S_5 is 2.88° delayed in relation to S_1. Since S_5 and S_7 are 180° phase shifted, the sum of this mismatch with the value of D_0 is shown in Figure 9 (c), thus making a total phase lag of 182.88° between S_1 and S_7. As expected, the triggering gate signals of S_2, S_4, S_6, and S_8 are complementary to the ones presented in Figure 9.

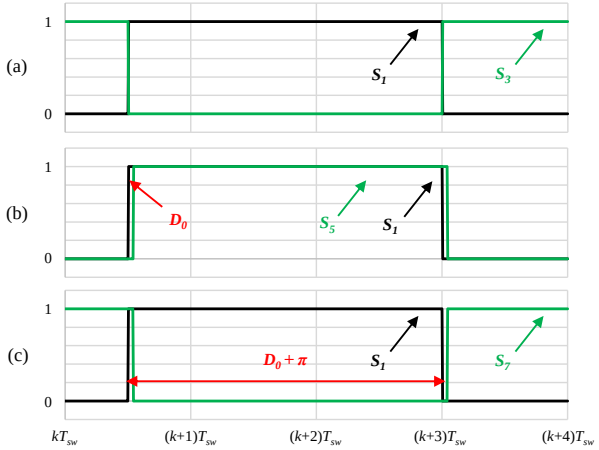

Figure 9. Triggering gate signals using SPS modulation: (a) S_1, S_3; (b) S_1, S_5; (c) S_1, S_7.

3.3. Dual Phase Shift (DPS)

Compared to SPS, the DPS modulation contemplates two degrees of freedom (D_0 and D_1). With the inclusion of D_1, the DAB converter presents greater flexibility and efficiency since reactive power, circulating currents, and current peaks may be compensated. By adding an equal phase mismatch between the legs of each H-bridge (D_1), v_{pri} and v_{sec} will be generated with three voltage levels ($+v_{dcx}$, 0, and $-v_{dcx}$), which contributes to increase the efficiency of the HF transformer and lower the THD.

Additionally, and as expected, the higher the values of D_0 and D_1, the greater the transferred power to and from

each side of the DAB converter. Thus, in Figure 10 (a) and Figure 10 (b) it is observed, respectively, the evolution of the transferred power as a function of the phase angles D_0 and D_1. In the first case, D_0 varies, once again, from 0 to $\pi/2$ rad, while D_1 assumes a fixed value of $\pi/3$ rad. On the other hand, when D_1 varies from 0 to π rad, D_0 assumes a fixed value of $\pi/9$ rad. Compared to SPS modulation, the value of D_0 for which P_N is reached is much higher (for the given value of D_1), sensibly around $5\pi/12$ rad ($\approx 75°$). On the other hand, when D_1 varies and D_0 is fixed, P_N is reached at approximately $8\pi/9$ rad ($\approx 160°$).

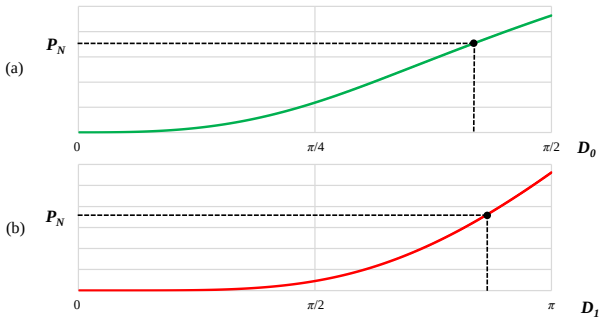

Figure 10. DAB power transfer during DPS modulation considering an increase of: (a) D_0; (b) D_1.

Regarding the DAB operating parameters, the values of D_0 and D_1 are calculated based on duty-cycle and phase shift modulations. As for the SPS case, D_0 is obtained by applying a PI algorithm to control v_{dc2}, whereas D_1 is determined with (2) and (3). As it is possible to conclude, D_1 will vary dynamically in accordance with the ratio between v_{dc1} and v_{dc2}, being as much smaller as the value of this ratio. Moreover, D_{1max} is representative of the maximum value that D_1 can assume, while k is a gain that may be adjusted according to the desired performance for the control algorithm.

$$error = \left| n - \frac{v_{dc1}}{v_{dc2}} \right| \tag{2}$$

$$D_1 = D_{1_{max}}\, e^{-k\, error} \tag{3}$$

As for SPS modulation, in Figure 11 are shown the triggering gate signals of semiconductors S_1, S_3, S_5, and S_7 when a DPS modulation is applied. As it can be seen in Figure 11 (a), the phase mismatch between S_1 and S_3 is the value of D_1, the value of D_0 is, once again, applied between S_1 and S_5 (Figure 11 (b)), while S_1 and S_7 are lagged $D_0 + D_1$ rad (Figure 11 (c)).

Since S_3, S_5, and S_7 lag S_1, it is proven the power flow direction in the DAB converter, i.e., from the primary to the secondary side. This fact can also be confirmed by analyzing the voltage waveforms of v_{pri} and v_{sec} in Figure 12 (a), the latter being delayed from the former.

In turn, Figure 12 (b) shows the waveforms of i_{pri} and i_{sec} by applying a DPS modulation to the DAB converter. Although the currents do not assume zero value when the v_{pri} and v_{sec} do, their mean value is null. Compared to SPS, the peak value of i_{pri} and i_{sec} is sensibly the double, however the reactive power and semiconductor stress will be much lower (in steady-state, for the same operating power, the RMS current value is also the same).

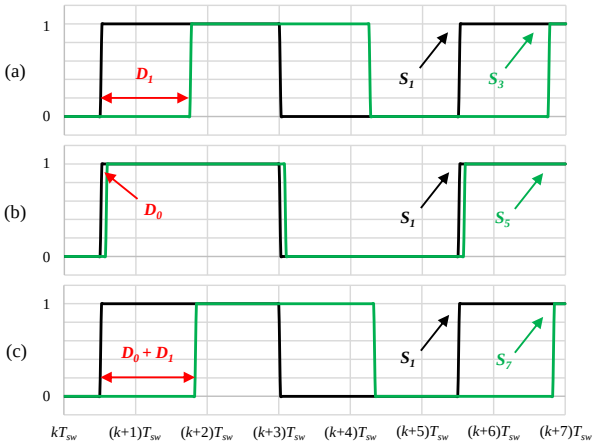

Figure 11. Triggering gate signals using DPS modulation: (a) S_1, S_3; (b) S_1, S_5; (c) S_1, S_7.

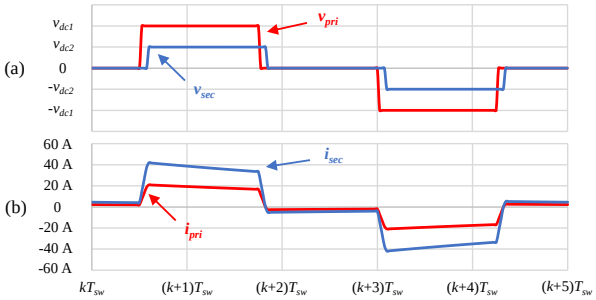

Figure 12. Waveforms in the primary and secondary sides of the HF transformer when the DAB operates under DPS modulation: (a) Voltage; (b) Current.

By observing Figure 12 (a), it can also be concluded that the steady-state value of v_{dc2} is sensibly 200 V. However, in Figure 13, it is presented the regulation of v_{dc2} at a transient state, occurring, in the instant $t = (k+2)T_{sw}$, the operation start of the secondary bridge switching signals. Thus, a pre-charge of the dc-link capacitors is carried out, which avoids overcurrent and reduces P_t. The steady-state value of v_{dc2}, as observed in detail, is 199.6 V.

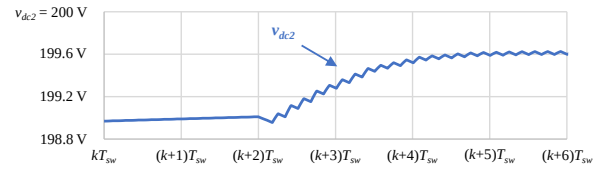

Figure 13. Secondary dc-link voltage (v_{dc2}) regulation considering a DPS modulation.

3.4. Extended Phase Shift (EPS)

As above-mentioned, EPS is considered the most suitable modulation technique for application in medium/high

power scenarios. When compared to SPS, EPS is capable of reducing circulating currents and P_{cond} when it is intended to transfer high power values to and from each side of the DAB. In addition, the soft-switching capacity of the converter is improved and the ZVS operation range may be largely extended.

In turn, in low power systems and under light load conditions, EPS modulation may even provoke worst results than SPS, since it is expected higher current peaks and semiconductor stress. Compared to DPS modulation, the main difference lies in the triggering gate signal of S_7. Once again, two degrees of freedom are considered (D_0 and D_1), with S_3 being D_1 rad ahead of S_1 (Figure 14 (a)), S_5 being D_0 rad ahead of S_1 (Figure 14 (b)), and S_7, instead of being the result of the sum of D_0 and D_1, is complementary to S_5 (Figure 14 (c)).

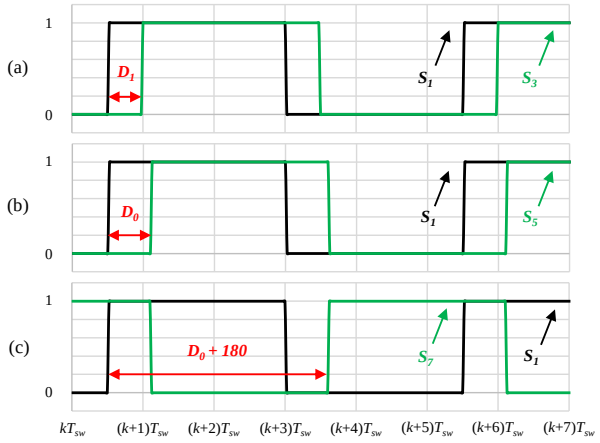

Figure 14. Triggering gate signals using EPS modulation: (a) S_1, S_3; (b) S_1, S_5; (c) S_1, S_7.

Given the triggering gate signals applied to each switching device, and as observed in Figure 15 (a), v_{pri} and v_{sec} present waveforms with a different number of voltage levels, the former considering three levels (v_{dc1}, 0, and $-v_{dc1}$) and the latter only two (v_{dc2} and $-v_{dc2}$). During time instants t_1, t_2, and t_3, since v_{pri} and v_{sec} assume their absolute maximum value with opposed polarities at the same time (±400 V and ±200 V, respectively), i_{pri} and i_{sec} increase more sharply, thus resulting in incompatible peak values (Figure 15 (b)). Besides, and as expected, the mean value of i_{pri} and i_{sec} is, once again, null.

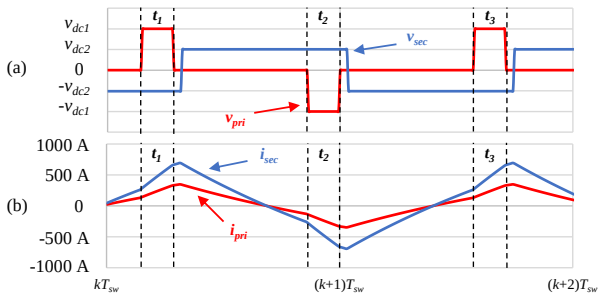

Figure 15. Waveforms in the primary and secondary sides of the HF transformer when the DAB operates under EPS modulation: (a) Voltage; (b) Current.

To reduce such current peaks, the value of D_1 or D_0 could be increased, however, the control of v_{dc2} would be impossible to be achieved. On the other hand, the value of L_k or f_{sw} could also be increased. Notwithstanding, and as previously defined in Table 1, the parameters of the DAB converter must be maintained constant throughout all the modulation techniques.

As for the previously explained modulation techniques, in Figure 16, it is shown the regulation of v_{dc2} during a transient state, once again coincident with the enabling of the switching operation in the secondary H-bridge of the DAB converter. As observed, the steady-state value of v_{dc2} is fixed at 202.7 V, thus resulting in a 2.7 V difference regarding the pre-established reference (200 V).

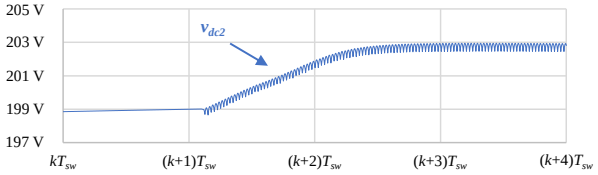

Figure 16. Secondary dc-link voltage (v_{dc2}) regulation considering an EPS modulation.

3.5. Triple Phase Shift (TPS)

In the literature, among the five modulation techniques analyzed in this paper, TPS is considered the one that presents the best energy efficiency and power quality results. With the inclusion of the third degree of freedom (D_2), the flexibility of the control algorithms is expanded, thus resulting in circulating currents mitigation, reactive power compensation, and semiconductor stress reduction. Since all the phase angles (D_0, D_1, and D_2) are independent of each other, the implementation difficulty of the TPS modulation is increased, which justifies its lower frequency of use in DAB converters. Moreover, given the relatively higher value of the cost-benefit ratio presented by the DPS modulation, TPS is in most cases disregarded.

As above-mentioned, in the cases of SPS and EPS modulation, the triggering gate signal applied to S_7 results from the sum of D_0 with π. For DPS modulation, it is considered the sum of D_0 with D_1. However, as mentioned in the literature, the non-existence of the third degree of freedom (D_2, applied between the legs of the secondary H-bridge) limits the optimization of the soft-switching capacity and the expansion of the ZVS range. In turn, and as observed in Figure 17 (c), for TPS modulation, the triggering gate signal of S_7 results from the sum of D_0 with D_2. Figure 17 (a) and Figure 17 (b) show the triggering gate signals applied to S_1, S_3, and S_5 in steady-state, considered quite similar to the ones applied during EPS and DPS, being added the value of D_1 and D_0, respectively, to the reference of S_1.

Since D_2 does not possess a preponderant role in the power value to be transferred through the DAB (it is only included to increase the converter efficiency), its value was varied manually, i.e., without applying any control

strategy. For this reason, contrarily to what was presented in sections referring to SPS (section 3.2.) and DPS (section 3.3.), the graphic representing the evolution of the transferred power as a function of the phase angles (D_0, D_1, and D_2) is not shown. Nevertheless, in situations where it is addressed the expansion of the ZVS range, D_2 must be calculated based on appropriate control strategies.

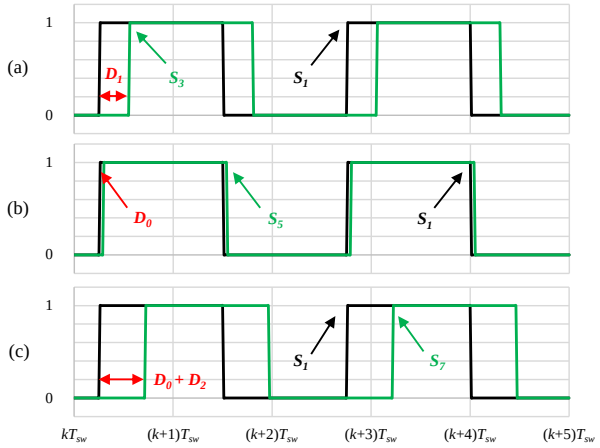

Figure 17. Triggering gate signals using TPS modulation: (a) S1, S3; (b) S1, S5; (c) S1, S7.

Through the analysis of Figure 18, it is concluded that the addition of D_2 increases, indeed, the flexibility of the control algorithm. By varying the duty-cycle of D_2, the TPS modulation may be applied in low power systems, which was not the case with EPS. As seen in Figure 18 (a), the adjustment of D_2 changes the time that v_{sec} assumes its absolute maximum value (around 200 V), which will have a slight consequence on the power transfer. However, the variation of D_2 has a more pronounced consequence on the reactive power produced by the DAB, which can be confirmed by observing the waveforms of i_{pri} and i_{sec} in Figure 18 (b). As with DPS modulation, i_{pri} and i_{sec}, despite having, respectively, peak values of 25 A and 50 A and not assuming instantaneous zero value when v_{pri} and v_{sec} do, present null mean value. Thus, semiconductor stress may be lower and the efficiency slightly higher.

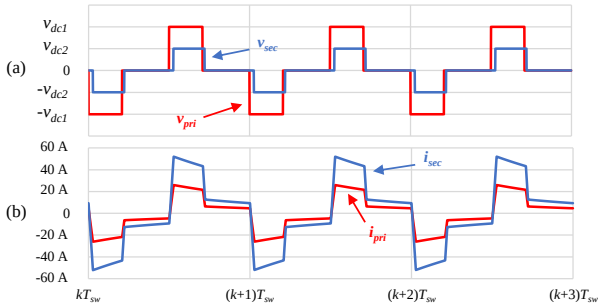

Figure 18. Waveforms in the primary and secondary sides of the HF transformer when the DAB operates under TPS modulation: (a) Voltage; (b) Current.

In Figure 19, it is shown the control of v_{dc2}, being possible to observe the instant in which the switching of the DAB's secondary H-bridge is enabled. This measure, as for the DPS case, has the objective to perform a pre-charge of the dc-link capacitors, consequently reducing P_t. In steady-state, the value of v_{dc2} is fixed at 199.7 V, only 0.3 V apart from the pre-established reference of 200 V.

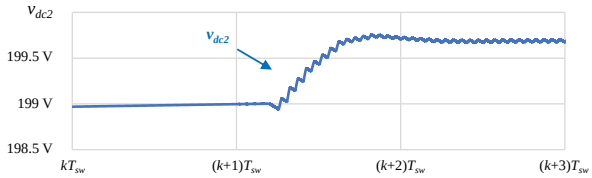

Figure 19. Secondary dc-link voltage (v_{dc2}) regulation considering a TPS modulation.

4. Conclusions

This paper studied and compared, by means of computer simulations, five modulation techniques capable of being applied to a dual active bridge (DAB) converter, namely Duty-Cycle Modulation, Single Phase Shift (SPS), Dual Phase Shift (DPS), Extended Phase Shift (EPS), and Triple Phase Shift (TPS). For all the cases, there were presented the voltage and current waveforms in the primary and secondary sides of the DAB high-frequency transformer, the triggering gate signals applied to the semiconductors S_1, S_3, S_5, and S_7, and the voltage waveform in the DAB secondary dc-link (v_{dc2}). To assess which modulation technique was more adequate for this particular operation case, the DAB parameters were maintained constant throughout all the simulations. Thus, the results were obtained for an operating power of 3.6 kW and a switching frequency (f_{sw}) of 100 kHz. Among the five studied modulation techniques, it was concluded that only the SPS, DPS and TPS are suitable for this case. When the converter operates as a single active bridge (SAB) under duty-cycle modulation, limitations regarding power transfer arise. On the other hand, the EPS modulation causes high current peaks in each side of the high-frequency transformer, which could be mitigated by increasing the value of f_{sw} or the DAB leakage inductance. Moreover, the values of the inner phase angle D_1 or the outer phase angle D_0 could also be increased to mitigate such current peaks, however, the regulation of v_{dc2} would be compromised. Thus, given the fixed DAB operating parameters, the EPS was considered more suitable for medium/high power and dynamic systems. Comparing the SPS, DPS and TPS, the last one proved to be the most flexible modulation, since three degrees of freedom are enabled, while the SPS presents only one, and the DPS two. However, the TPS implementation difficulty is much higher than in the other modulation techniques, which justifies its lower utilization. On the other hand, the DPS is the most referred modulation, since it presents a higher cost-benefit ratio. Moreover, when the DAB input voltage does not match the multiplication of the transformation ratio by v_{dc2}, the DPS is capable of mitigating the reactive power and the

circulating currents, which is not the case for the SPS modulation.

Acknowledgements.

This work has been supported by FCT (Fundação para a Ciência e Tecnologia) within the Project Scope: UIDB/00319/2020. This work has been supported by the FCT Project PV4SUSTAINABILITY Ref. 333203230 and by the project newERA4GRIDs Ref. PTDC/EEIEEE/30283/2017. Tiago J. C. Sousa is supported by the doctoral scholarship SFRH/BD/134353/2017 granted by FCT.

References

[1] R. W. A. A. de Doncker, D. M. Divan, and M. H. Kheraluwala, "A Three-Phase Soft-Switched High-Power-Density DC/DC Converter for High-Power Applications," *IEEE Transactions on Industry Applications*, vol. 27, no. 1, pp. 63–73, 1991.

[2] S. Chakraborty and S. Chattopadhyay, "Fully ZVS, Minimum RMS Current Operation of the Dual-Active Half-Bridge Converter Using Closed-Loop Three-Degree-of-Freedom Control," *IEEE Transactions on Power Electronics*, vol. 33, no. 12, pp. 10188–10199, 2018.

[3] L. Roggia, L. Schuch, J. E. Baggio, C. Rech, and J. R. Pinheiro, "Integrated full-bridge-forward dc-dc converter for a residential microgrid application," *IEEE Transactions on Power Electronics*, vol. 28, no. 4, pp. 1728–1740, 2013.

[4] J. A. Mueller and J. W. Kimball, "Modeling Dual Active Bridge Converters in DC Distribution Systems," *IEEE Transactions on Power Electronics*, vol. 34, no. 6, pp. 5867–5879, 2019.

[5] L. Zheng, R. P. Kandula, and D. Divan, "Soft-Switching Solid-State Transformer with Reduced Conduction Loss," *IEEE Transactions on Power Electronics*, vol. 36, no. 5, pp. 5236–5249, 2021.

[6] B. Chen, X. Liang, and N. Wan, "Design Methodology for Inductor-Integrated Litz-Wired High-Power Medium-Frequency Transformer with the Nanocrystalline Core Material for Isolated DC-Link Stage of Solid-State Transformer," *IEEE Transactions on Power Electronics*, vol. 35, no. 11, pp. 11557–11573, 2020.

[7] M. Nazmunnahar, S. Simizu, P. R. Ohodnicki, S. Bhattacharya, and M. E. McHenry, "Finite-Element Analysis Modeling of High-Frequency Single-Phase Transformers Enabled by Metal Amorphous Nanocomposites and Calculation of Leakage Inductance for Different Winding Topologies," *IEEE Transactions on Magnetics*, vol. 55, no. 7, 2019.

[8] N. D. Dao, D. C. Lee, and Q. D. Phan, "High-Efficiency SiC-Based Isolated Three-Port DC/DC Converters for Hybrid Charging Stations," *IEEE Transactions on Power Electronics*, vol. 35, no. 10, pp. 10455–10465, 2020.

[9] D. Wang, B. Nahid-Mobarakeh, and A. Emadi, "Second harmonic current reduction for a battery-driven grid interface with three-phase dual active bridge DC-DC converter," *IEEE Transactions on Industrial Electronics*, vol. 66, no. 11, pp. 9056–9064, 2019.

[10] R. Agarwal, S. Martin, and H. Li., "Influence of Phase-Shifted Square Wave Modulation on Medium Frequency Transformer in a MMC Based SST," *IEEE Access*, 2020.

[11] J. Liu, J. Yang, J. Zhang, Z. Nan, and Q. Zheng, "Voltage Balance Control Based on Dual Active Bridge DC/DC Converters in a Power Electronic Traction Transformer," *IEEE Transactions on Power Electronics*, vol. 33, no. 2, pp. 1696–1714, 2018.

[12] J. Hu, P. Joebges, G. C. Pasupuleti, N. R. Averous, and R. W. de Doncker, "A Maximum-Output-Power-Point-Tracking-Controlled Dual-Active Bridge Converter for Photovoltaic Energy Integration into MVDC Grids," *IEEE Transactions on Energy Conversion*, vol. 34, no. 1, pp. 170–180, 2019.

[13] B. Kwak, M. Kim, and J. Kim, "Inrush current reduction technology of DAB converter for low-voltage battery systems and DC bus connections in DC microgrids," *IET Power Electronics*, vol. 13, no. 8, pp. 1528–1536, 2020.

[14] P. Liu, C. Chen, and S. Duan, "An optimized modulation strategy for the three-level DAB converter with five control degrees of freedom," *IEEE Transactions on Industrial Electronics*, vol. 67, no. 1, pp. 254–264, 2020.

[15] Y. Xuan, X. Yang, W. Chen, T. Liu, and X. Hao, "A novel NPC dual-active-bridge converter with blocking capacitor for energy storage system," *IEEE Transactions on Power Electronics*, vol. 34, no. 11, pp. 10635–10649, 2019.

[16] Y. P. Chan, M. Yaqoob, C. S. Wong, and K. H. Loo, "Realization of High-Efficiency Dual-Active-Bridge Converter with Reconfigurable Multilevel Modulation Scheme," *IEEE Journal of Emerging and Selected Topics in Power Electronics*, vol. 8, no. 2, pp. 1178–1192, 2020.

[17] J. Wu, Y. Li, X. Sun, and F. Liu, "A new dual-bridge series resonant DC-DC converter with dual tank," *IEEE Transactions on Power Electronics*, vol. 33, no. 5, pp. 3884–3897, 2018.

[18] M. Rolak, C. Sobol, M. Malinowski, and S. Stynski, "Efficiency Optimization of Two Dual Active Bridge Converters Operating in Parallel," *IEEE Transactions on Power Electronics*, vol. 35, no. 6, pp. 6523–6532, 2020.

[19] K. Takagi and H. Fujita, "Dynamic Control and Performance of a Dual-Active-Bridge DC-DC Converter," *IEEE Transactions on Power Electronics*, vol. 33, no. 9, pp. 7858–7866, 2018.

[20] P. Xia, H. Shi, H. Wen, Q. Bu, Y. Hu, and Y. Yang, "Robust LMI-LQR Control for Dual-Active-Bridge DC-DC Converters with High Parameter Uncertainties," *IEEE Transactions on Transportation Electrification*, vol. 6, no. 1, pp. 131–145, 2020.

[21] N. Vazquez and M. Liserre, "Peak current control and feed-forward compensation of a DAB converter," *IEEE Transactions on Industrial Electronics*, vol. 67, no. 10, pp. 8381–8391, 2020.

[22] O. M. Hebala, A. A. Aboushady, K. H. Ahmed, and I. Abdelsalam, "Generic Closed-Loop Controller for Power Regulation in Dual Active Bridge DC-DC Converter With Current Stress Minimization," *IEEE Transactions on Industrial Electronics*, vol. 66, no. 6, pp. 4468–4478, 2019.

[23] M. Yaqoob, K. H. Loo, and Y. M. Lai, "A four-degrees-of-freedom modulation strategy for dualactive- bridge series-resonant converter designed for total loss minimization," *IEEE Transactions on Power Electronics*, vol. 34, no. 2, 2019.

[24] P. Liu and S. Duan, "A Hybrid Modulation Strategy Providing Lower Inductor Current for the DAB Converter with the Aid of DC Blocking Capacitors," *IEEE Transactions on Power Electronics*, vol. 35, no. 4, pp. 4309–4320, 2020.

[25] Z. Qin, Y. Shen, P. C. Loh, H. Wang, and F. Blaabjerg, "A Dual Active Bridge Converter with an Extended High-Efficiency Range by DC Blocking Capacitor Voltage Control," *IEEE Transactions on Power Electronics*, vol. 33, no. 7, pp. 5949–5966, 2018.

[26] G. Xu, D. Sha, Y. Xu, and X. Liao, "Hybrid-Bridge-Based DAB Converter with Voltage Match Control for Wide Voltage Conversion Gain Application," *IEEE Transactions on Power Electronics*, vol. 33, no. 2, pp. 1378–1388, 2018, doi: 10.1109/TPEL.2017.2678524.

[27] A. Garcia-Bediaga, I. Villar, A. Rujas, and L. Mir, "DAB modulation schema with extended ZVS region for applications with wide input/output voltage," *IET Power Electronics*, vol. 11, no. 13, 2018.

[28] Y. Xiao, Z. Zhang, M. A. E. Andersen, and K. Sun, "Impact on ZVS Operation by Splitting Inductance to Both Sides of Transformer for 1-MHz GaN Based DAB Converter," *IEEE Transactions on Power Electronics*, vol. 35, no. 11, pp. 11988–12002, 2020.

[29] N. A. Dung, H. J. Chiu, J. Y. Lin, Y. C. Hsieh, and Y. C. Liu, "Efficiency optimisation of ZVS isolated bidirectional DAB converters," *IET Power Electronics*, vol. 11, no. 8, pp. 1–8, 2018.

[30] G. Xu, D. Sha, Y. Xu, and X. Liao, "Dual-Transformer-Based DAB Converter with Wide ZVS Range for Wide Voltage Conversion Gain Application," *IEEE Transactions on Industrial Electronics*, vol. 65, no. 4, pp. 3306–3316, 2018.

[31] T. Dai *et al.*, "Research on Transient DC Bias Analysis and Suppression in EPS DAB DC-DC Converter," *IEEE Access*, vol. 8, pp. 61421–61432, 2020.

[32] Q. Bu, H. Wen, J. Wen, Y. Hu, and Y. Du, "Transient DC bias elimination of dual-active-bridge DC-DC converter with improved triple-phase-shift control," *IEEE Transactions on Industrial Electronics*, vol. 67, no. 10, pp. 8587–8598, 2020.

[33] F. Wu, F. Feng, and H. B. Gooi, "Cooperative Triple-Phase-Shift Control for Isolated DAB DC-DC Converter to Improve Current Characteristics," *IEEE Transactions on Industrial Electronics*, vol. 66, no. 9, pp. 7022–7031, 2019.

[34] S. Luo, F. Wu, and G. Wang, "Improved TPS control for DAB DC-DC converter to eliminate dual-side flow back currents," *IET Power Electronics*, vol. 13, no. 1, pp. 32–39, 2020.

[35] X. Liu *et al.*, "Novel Dual-Phase-Shift Control With Bidirectional Inner Phase Shifts for a Dual-Active-Bridge Converter Having Low Surge Current and Stable Power Control," *IEEE Transactions on Power Electronics*, vol. 32, no. 5, pp. 4095–4106, 2017.

[36] N. Hou, W. Song, Y. Li, Y. Zhu, and Y. Zhu, "A Comprehensive Optimization Control of Dual-Active-Bridge DC-DC Converters Based on Unified-Phase-Shift and Power-Balancing Scheme," *IEEE Transactions on Power Electronics*, vol. 34, no. 1, pp. 826–839, 2018.

[37] N. Fritz, M. Rashed, S. Bozhko, F. Cuomo, and P. Wheeler, "Flux Control Modulation for the Dual Active Bridge DC / DC Converter," pp. 1–6.

[38] S. Zengin and M. Boztepe, "A Novel Current Modulation Method to Eliminate Low-Frequency Harmonics in Single-Stage Dual Active Bridge AC-DC Converter," *IEEE Transactions on Industrial Electronics*, vol. 67, no. 2, pp. 1048–1058, 2020.

[39] I. Kayaalp, T. Demirdelen, T. Koroglu, M. U. Cuma, K. C. Bayindir, and M. Tumay, "Comparison of Different Phase-Shift Control Methods at Isolated Bidirectional DC-DC Converter," *International Journal of Applied Mathematics, Electronics and Computers*, vol. 4, no. 3, p. 68, 2016.

[40] A. Kumar, A. H. Bhat, and P. Agarwal, "Comparative Analysis of Dual Active Bridge Isolated DC to DC Converter with Double Phase Shift and Triple Phase Shift Control Techniques," *2017 Recent Developments in Control, Automation and Power Engineering, RDCAPE 2017*, vol. 3, pp. 257–262, 2017.